Nano Research
2019, 12(7): 1635–1642

ISSN 1998-0124 CN 11-5974/O4
https://doi.org/10.1007/s12274-019-2412-x

Research Article

Oxidation controlled lift-off of 3D chiral plasmonic Au nano-hooks

Gunnar Klös[1], Amanda Andersen[1,2], Matteo Miola[1,3], Henrik Birkedal[1,2], and Duncan S. Sutherland[1] (✉)

[1] *Interdisciplinary Nanoscience Center (iNANO), Aarhus University, Aarhus C 8000, Denmark*
[2] *Department of Chemistry and iNANO, Aarhus University, Aarhus C 8000, Denmark*
[3] *Carbon Dioxide Activation Center (CADIAC) - iNANO, Aarhus University, Aarhus C 8000, Denmark*

Received: 14 January 2019 / **Revised:** 8 April 2019 / **Accepted:** 9 April 2019

ABSTRACT

Colloidal suspensions of plasmonic nanoparticles (NPs) are a well-established tool for biomedical applications and enhanced spectroscopy because of their strong optical response. The specific response is greatly dependent on the NP shape. The strong optical activity of chiral NPs has created special interest but fabrication of chiral NPs in solution remains challenging. Here, we present an approach whereby three-dimensional (3D) chiral Au nano-hooks, fabricated with the parallel hole-mask colloidal lithography (HMCL) method, can be lifted off from a glass substrate in a controllable manner by using a combined treatment with oxygen plasma oxidation and a reduction step in solution. This method has the advantage of being based on established techniques and not requiring strong acids or complex substrates as in etching based approaches. We furthermore demonstrate the integration of the hook NPs into reversibly cross-linked hydrogels inspired by mussel catechol chemistry but containing an oxidation resistant catechol analogue grafted onto poly(allylamine) crosslinked by coordination of Al^{3+} and how this facilitates the remote analysis of hydrogel microenvironment, e.g. the water content. The suspended particles are promising candidates for optically active surface-enhanced Raman spectroscopy (SERS), asymmetric photo catalysis or aggregation sensing. The integration into hydrogels to produce functional hydrogels holds benefits for applications of metamaterials in optics, sensing or activation in environmental remediation or drug delivery.

KEYWORDS

chiral nanostructures, circular dichroism, plasmonic sensor, hole-mask colloidal lithography, lift-off

1 Introduction

The interaction of light with small metal nanoparticles (NPs) can excite collective oscillations of conduction electrons, known as localized surface plasmon resonance (LSPR), and give rise to various remarkable properties such as enhancement of optical transitions and non-local dielectric responses [1–3]. Especially for applications in chemistry, colloidal suspensions of NPs have the advantage of high surface area-to-volume ratios and surface accessibility, improving surface bonding properties and chemical reactivity [4–7].

The standard approach to fabricate suspended plasmonic NPs is to use solution-based synthesis, allowing for the high-yield production of mono-crystalline particles [8]. Although recent developments of synthesis techniques have resulted in an increased control over the geometry of NPs that can be generated, the obtainable NP shapes are very limited compared to lithographic techniques such as electron beam lithography (EBL) [9–11]. Since the optical properties of plasmonic NPs are strongly dependent on the particles shape, it is of great interest to precisely control this parameter and achieve highly monodisperse particles [12–14]. For achieving geometries that are more complex and especially the fabrication of anisotropic particles, the utilization of assembly techniques to form clusters of colloidal NPs has gained much interest [15–18]. Apart from the generation of hotspots, the more complex geometries of NP clusters also lead to the emergence of different interactions with light. In particular, chiral structures, that are not superimposable with their mirror image, show strong optical activity like circular dichroism (CD) and optical rotary dispersion (ORD) [19, 20].

Chiral NPs are employed in a broad range of applications, ranging from nano-sensors and -photonics to catalysis and more general nanoelectromechanical systems [21–26]. These applications demonstrate the great potential of suspended chiral NPs and pose the challenge to develop methods for the reliable fabrication with a high control over the particles shape. The solution-based synthesis of chiral NPs usually relies on assembly processes guided by chiral organic templates [27, 28]. Relying on templates limits the control over the NPs chirality, which is why more common approaches to fabricate chiral plasmonic nano-structures are usually based on lithographic techniques such as direct write EBL, allowing for highly precise and controllable structuring of two-dimensional (2D) and three-dimensional (3D) chiral NPs on a surface [29, 30]. These methods come with the drawback of being very costly and time consuming, with yields much lower than for solution-based synthesis. An alternative is given by large-area patterning techniques like nano-imprint lithography (NIL) based on EBL defined imprint masks or colloidal lithography (CL) [31, 32]. The latter uses colloidal suspensions to form self-assembled layers for the patterning of some cm^2 surface areas [32]. To achieve suspensions of the nano structures fabricated with lithographic approaches, the NPs have to be lifted-off from the surface, a process that usually involves strong etchants followed by purification steps [33–35].

Here, we report a novel way of generating colloidal suspensions of chiral plasmonic NPs by using hole-mask colloidal lithography (HMCL) for the fabrication of specific chiral Au nano-hooks with a tunable CD response in the visible and near-infrared (NIR) and lifting them off the substrate by a combined treatment with oxygen plasma

Address correspondence to duncan@inano.au.dk

and reducing solutions. HMCL enables the large-scale and low-cost fabrication of monodisperse 3D NPs with a high control over the NPs shape and size [35–39]. Using a 3D chiral Au nano-hook structure we demonstrate how HMCL can be used to precisely tune the CD response of chiral NPs in the visible and NIR. The structures are then transferred into either an ethanol or an aqueous solution at neutral pH, a process controlled by a prior treatment with strong oxygen plasma. Lastly, we demonstrate how NP suspensions can be incorporated into hydrogels and for the first time, to our knowledge, realizing such incorporation for a supramolecular, reversibly cross-linked hydrogel [40–42]. To this end we use a construct based on the strong coordination between Al(III) ions and an oxidation resistant catechol analogue (cHOPO, (1-(2′carboxyethyl)-2-methyl-3-hydroxy-4(1H)-pyri-dinone) grafted onto polyallylamine (g-cHOPO-PAH) [43]. Furthermore, we show how the integrated NPs allow the remote and dynamic sensing of the hydrogels water content. The chirality of the hook structure enables the use of CD measurements for this sensing, which requires a lower NP concentration than necessary for direct extinction measurements.

Having precise control over the exact shape and optical activity of suspended NPs holds great potential exploring many effects like superchirally driven asymmetric photocatalysis or interactions with chiral molecules for pharmaceutical and biological applications [19, 44]. In particular, the demonstrated incorporation of such NPs into hydrogel holds potential for applications in environmental remediation or drug delivery, especially in the case of the Al(III): g-cHOPO-PAH construct with its reversible gelation and self-healing properties [43, 45–47].

2 Results and discussion

2.1 Fabrication and tunability of Au nano-hooks

Figure 1 schematically depicts the fabrication process for the Au nano-hooks, including the various tunable parameters. The fabrication is based on the low-cost and highly scalable technique of HMCL [36]. To achieve chiral structures with the achiral hole-mask, HMCL is used in combination with angled physical vapour deposition (PVD). This method allows simultaneously tilting and rotating the sample during the metal deposition process. Here, we used the prototype PVD machine Cryofox-GLAD from Polyteknik (Denmark), which allows free control of the tilt angle α and in-plane rotation angle β, during the deposition. Keeping α fixed while rotating the sample less than 360° leads to hook-like structures due to the clogging of the hole while depositing material [48, 49]. The radius R of the hooks is determined by α and the circular sectioning φ by β_{max} while the free control over β enables the precise modification of the width w and height H of the hook and their decrease along its backbone. This change in w and H is the origin of the hooks' chirality, and having precise control over these parameters allows tuning of its optical activity.

In Fig. 2, a comprehensive study of the influence of the hooks structural parameters on their CD optical activity is presented. For all presented structures, β was rotated from 0° to 270° at a deposition rate of 1 Å/s. The top row shows that varying the static parameters tilt α Fig. 2(a) and PS size S Fig. 2(b) enables a shift in the LSPR peak to higher or lower wavelengths in the visible and NIR for bigger and smaller angles α, respectively, and that increasing the particle size S leads to an increase in the intensity of the response. The shift of the resonance position is a result of the change of the NP's aspect ratio as well as of the influence of α on the length of the hooks' backbone: Modifying the distance the oscillating electrons are moving and thus the wavelength necessary to excite the oscillations. The latter only affects the CD signal, as can be seen in comparison to the unpolarized extinction spectra shown in Fig. S4 in the Electronic Supplementary Material (ESM). The increased intensity arises from the increased amount of material deposited due to the larger hole size, resulting in more conduction electrons contributing to the LSPR. The bottom row in Fig. 2 displays the effect the variation of the rotation β has on the CD signal. By making the rotation speed faster (C), the signal is reduced due to the smaller total amount of deposited material and the flatter profile of the hook.

The profile shape can be further varied by changing from constant rotation speed to an accelerated rotation (D, for atomic force microscopy (AFM) characterization see Fig. S1 in the ESM). In both modes the same total amount of material is deposited but in the latter mode the rotation speed is constantly increased from 29 s/° to 4 s/°, at which it was kept for the last 50° to ensure the formation of a coherent Au film in this part of the hook. The CD signal strongly increases and sharpens notably for the accelerated case, underlining the importance the 3D geometry of plasmonic NPs has on their optical response. We were able to show the versatility of the HMCL method for the fabrication of 3D chiral nano-structures and the high degree of tunability it allows in connection with sample tilt and rotation. This enables the fabrication of monodisperse structures on large areas in a low-cost and high-throughput manner. In the following section, a method for transferring the Au nano-hooks into a suspension is demonstrated, making this HMCL approach for

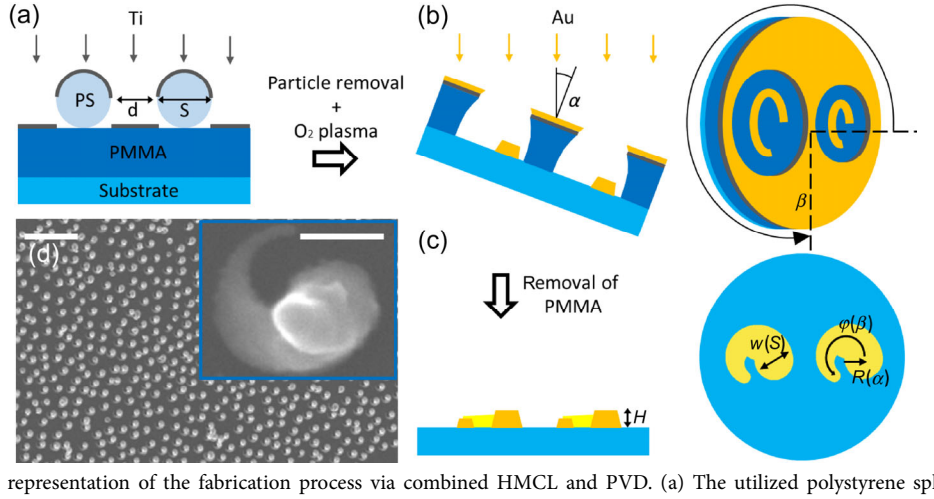

Figuer 1 (a)–(c) Schematic representation of the fabrication process via combined HMCL and PVD. (a) The utilized polystyrene sphere (PS) colloidal solution determines the hole size S and nearest-neighbor distance d. An etch-resistant mask is formed by a 20 nm thick Ti layer. (b) By controlling the sample tilt angle α and in-plane rotation angle β during the PVD process it is possible to precisely tune the structural parameters of the hook (height H, backbone radius R and circular sectioning φ, shown in (c) for the final sample after the cleaning procedure). The width w is determined by the PS size S. (d) SEM image of a nano-hook array, scale bar 1 μm. Inset: a single hook structure in high resolution, scale bar 100 nm.

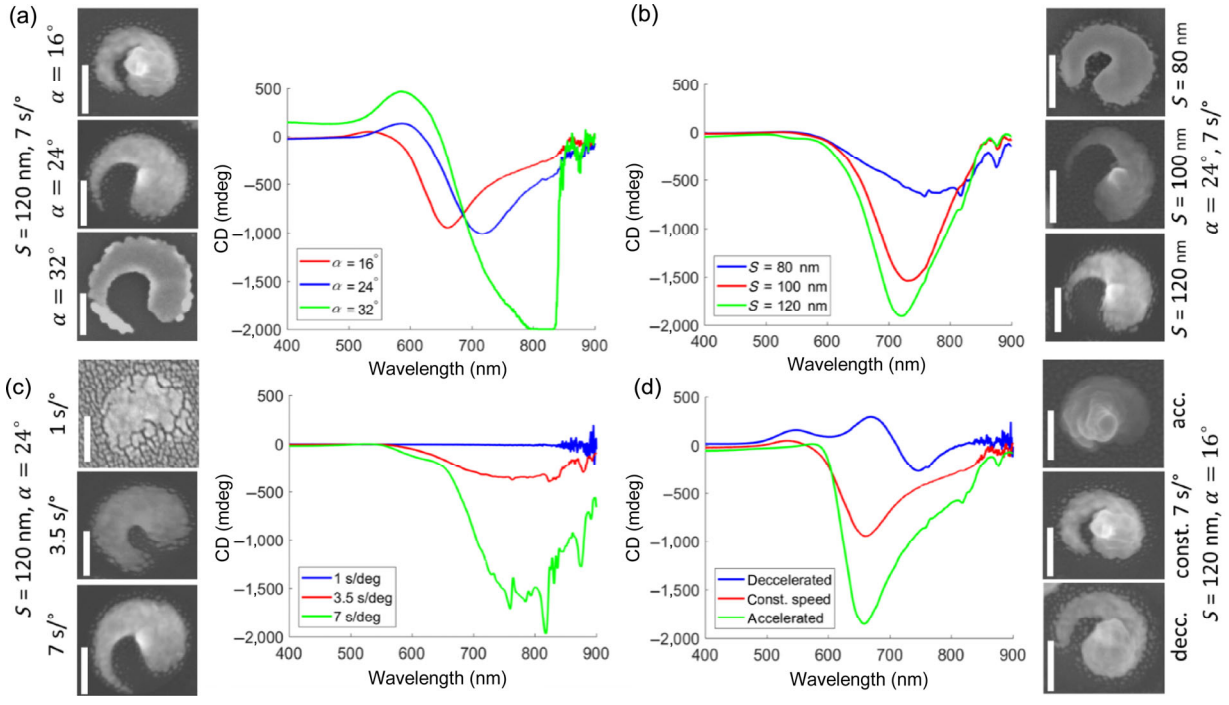

Figuer 2 Structure-plasmon relation of the nano-hook structure. The structural parameters varied as described in Fig. 1 and the structural change is verified using SEM images. The change in plasmon response is determined via CD spectra. (a) Increasing the tilt angle α and thus the backbone radius R red-shifts the plasmon peak. (b) Increasing the hook width w by using PS with larger size S slightly blue-shifts and strongly amplifies the peak. (c) Decreasing the rotation speed during the deposition process leads to smaller structures with less decrease in width w along the backbone. This entails a much lower LSPR response. (d) By changing from a constant rotation during the deposition process to an accelerated one, while keeping the total amount of deposited material constant, the hook gets a steeper height profile along its backbone. The result is a sharpened LSPR peak. All scale bars are 100 nm.

the fabrication of 3D chiral structures a viable tool for generating suspended NPs with complex geometries.

2.2 Lift-off

To transfer the hook NPs from the sample surface into a suspension a two-step process was performed. The first step was a prolonged O_2 plasma treatment (RF 100 W, 30 mbar pressure, 55 cm^3/s oxygen flow) that creates a stable layer of oxidized gold (Au(+3), see Fig. 5). This also affects the plasmon resonance, slightly red-shifting the peak positions, as shown in Fig. S5 in the ESM. The plasma treatment also leads to the removal of the Au nano-spots around the structures that are a result of surface diffusion and are a known problem in stencil lithography (see Fig. S1 in the ESM) [50].

The second step is the immersion of the sample in a solution with strong reducing agents, which leads to mobilization of the NPs and eventual lift-off. This is demonstrated for both, an aqueous solution with the strong ionic buffer HEPES (10 mM, 100 mM NaOH, pH 7.4) and for 1-dodecanethiols (10 mg/mL) in ethanol (> 99.5 vol.%). Figure S2 in the ESM highlights the necessity of the plasma oxidation step for a successful lift-off. The necessity of the reduction step is demonstrated in Fig. S6 in the ESM, which shows that ultrasonication of the oxidized sample in a non-reducing does not lead to lift-off.

In Fig. 3, the successful lift-off is characterized using CD spectroscopy and scanning electron microscopy. The top row compares the CD signal of the structures before lift-off on a glass substrate with the same structures in the ethanol-thiol solution (in a quartz cuvette, light path 1 mm) after having stored the plasma treated sample for 1 day in the solution followed by 1 min ultrasonication. Note that the CD LSPR peaks appear slightly red-shifted (on average 21 ± 9 nm, as calculated from the shown spectra), which can be attributed to either the change of refractive index (RI) from air (RI 1) to ethanol (RI 1.361) or to the change from a coherent direction of illumination to an average over illumination of all possible orientations due to the suspended state. The latter was verified by FDTD simulations (lumerical solutions, minimum feature size 2 nm), where the hooks CD spectra for various illumination directions were determined and then averaged, as displayed in Fig. 4(a). For the illumination normal to the hooks horizontal plane the FDTD simulations were also used to generate the differential E-field distribution (E-field for left-hand circular polarized, LCP illumination, minus E-field for right-hand circular polarized illumination, RCP) for the two major CD peaks, at 588 and 726 nm (Figs. 4(b) and 4(c)). At both wavelengths, quadrupole and higher order modes emerge with the higher wavelength experiencing stronger field enhancements, especially in the gap between the big and small end of the hook.

The scanning electron microscopy (SEM) images (Figs. 3(b)–3(e)) show the sample before and after a 2 h reduction in thiol solution ((b) and (c), no ultrasonication) as well as hooks that were redeposited from solution onto a Si wafer ((d) and (e)). The before and after image comparison clearly shows that the reduction step mobilizes the NPs on the surface; before reduction, all hooks have the same orientation and the ordering determined by the random sequential absorption of the PSs, while afterwards this pattern is broken with a strongly reduced surface coverage and a random orientation of the remaining hooks. Figure S2 in the ESM shows the similar situation for the samples in HEPES buffer and furthermore compares the samples with and without plasma oxidation, the latter showing no change in orientation or pattern, proving the necessity of the plasma treatment for a successful lift-off. A proposed explanation for this process is strain emerging in the hook upon reduction due to its highly asymmetrical shape. The SEM images of the redeposited hooks ((d) and (e)) confirm that the hooks maintain their chiral shape when lifted off the surface, as verified by the CD spectra, for both, the lift-off in aqueous and ethanol solutions. The aggregation visible in the SEM images could be attributed to the redeposition process, where the solution were left to dry on the Si wafer. This can lead to the so-called coffee-ring effect; to verify this assumption it would be necessary to suppress this effect, even though the CD

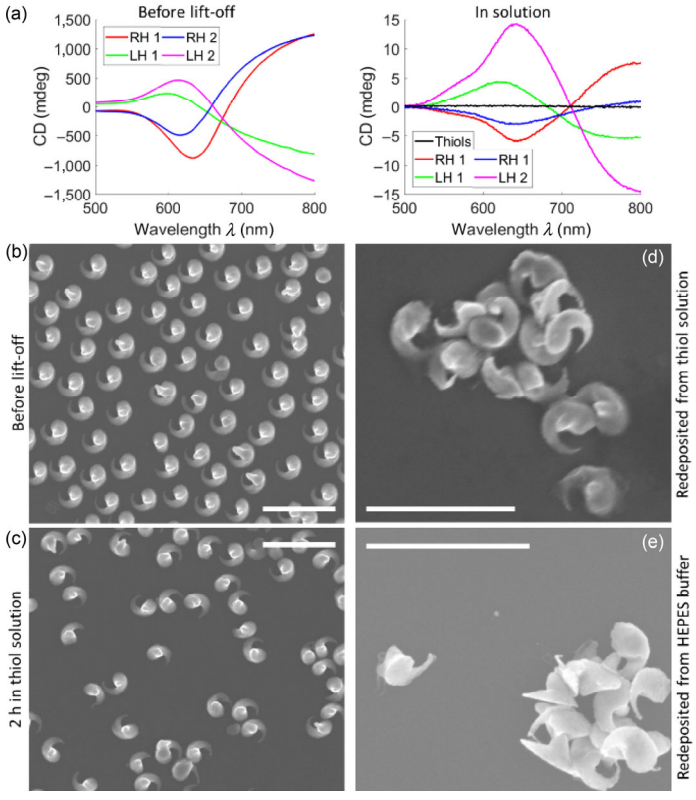

Figure 3 Verifying the successful particle lift-off. (a) Comparing the CD signal for two samples of each handedness before lift-off on the glass sample with those after lift-off, suspended in ethanol-thiol solution. The peak-shift results from the change in RI (1) from air to ethanol (1.361). SEM image of the hooks on a glass sample before (b) and after (c) the 2 h reduction in 10 mg/mL 1-dodecanethiols in ethanol. Reduction leads to mobilization of the nano-hooks as seen by the loss of order and decrease in surface coverage. Samples were covered in 4 nm Ti for imaging purposes. Nano-hooks redeposited on a Si wafer from suspension in thiol-solution (d) and HEPES buffer (e). The CD signal indicates that the apparent aggregation is a result of the redeposition and does not occur in the suspension. All scale bars are 500 nm.

spectra do not indicate aggregation of the suspended NPs [51, 52].

Successfully transferring lithographically designed NPs into suspension could hold further potential, e.g., for sensing application involving larger biomolecules or heterogeneous chemical catalysis, for which especially chiral NPs enable enhanced enantio-selectivity [53–55]. Furthermore, it allows the integration into hydrogels, which is demonstrated in the following section.

2.3 Hydrogel integration

To further explore the potential of suspended plasmonic particles we integrated the lift-off particles into two different hydrogels, gelatin and Al(III):g-cHOPO-PAH. Gelatin gels were cast by dissolving porcine gelatin at 10 wt.% in HEPES buffer at 55 °C in the NP suspension and then letting the solution cool down back to room temperature. The reversible Al(III):g-cHOPO-PAH hydrogel was fabricated by first dissolving 20 mg of the g-cHOPO-PAH ((1-(2′carboxyethyl)-2-methyl-3-hydroxy-4(1H)-pyridinone-grafted polyallylamine hydrochloride, synthesized by a previous published protocol) in 30 μL HEPES buffer, followed by adjustment of the pH to 7.4 by adding 10 μL of 5 M NaOH and further dilution with 100 μL of the colloidal suspension [43]. Reversible crosslinking was facilitated by the addition of 10 μL 0.5 mM aluminum chloride hexahydrate, which coordinates cHOPO above pH ~ 4 [43]. Before the hydrogel casting, the concentration of the hook solutions was increased by a factor of 4 by centrifugation (15 min, 15,000*g*) and removal of the top ¾ of liquid, followed by vortex mixing and ultrasonication.

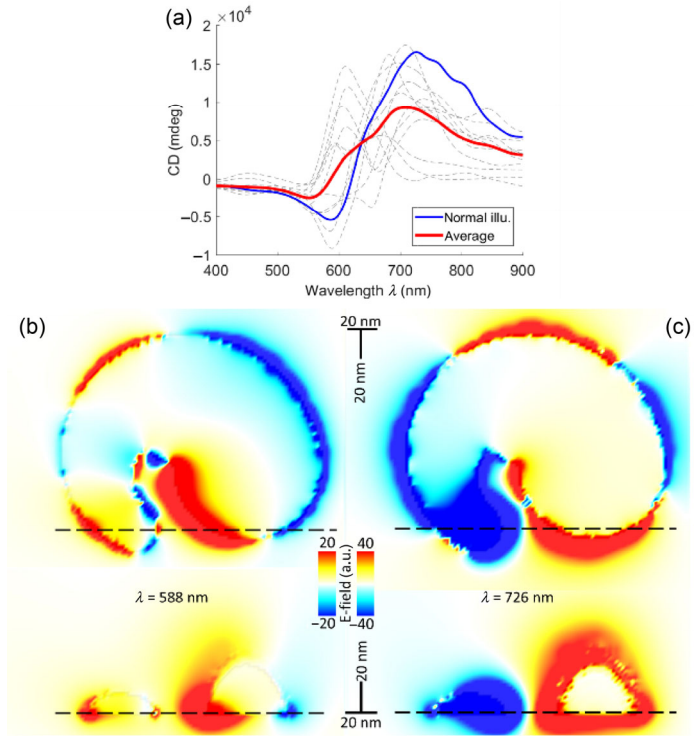

Figure 4 (a) Comparing the CD response of the hook under normal illumination and averaged over illumination from all directions (discretized to 45° angles) by FDTD simulations, which gives an additional explanation for the red-shift observed in Fig. 3. Differential E-field distribution (E_{RCP}-E_{LCP}) of the hook for wavelength λ = 588 nm (b) and λ = 726 nm (c), the minimum and maximum of the CD signal under normal illumination. Both wavelengths show the emergence of quadrupoles or higher order modes, with the higher wavelength having the stronger field enhancement, especially in the hook's gap. The dashed lines indicate the horizontal and vertical cross-section, respectively.

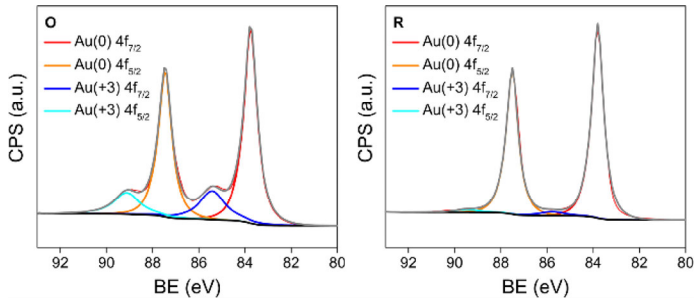

Figure 5 XPS spectra of the Au 4f peaks for a continuous, 20 nm thick gold film right after 12 min oxygen plasma treatment (O) and after reduction in HEPES buffer (R). In the former, the Au(+3) peaks at 85.4 and 89.1 eV, assigned to Au_2O_3 show a high level of oxidation [56–58].

The hydrogels, depicted in Fig. 6(a), were spectroscopically analyzed (Jasco-810 CD spectrometer for hooks on substrate, Chirascan CD spectrometer for hooks in solution and hydrogels and data, displayed in Fig. 6(b)). The spectra show that the NPs optical properties are well retained, both in gelatin and Al(III):g-cHOPO-PAH. Interestingly, upon lift-off and integration into the gel, the lower-wavelength CD peak changes signs. This can be explained by the simulations in Fig. 4(a), which show that the emergence of this peak strongly depends on the direction of illumination, specifically, it flips signs when changing from normal illumination to an average over all directions. The observable LSPR peak shift (measured for the lower-wavelength peak around 600 nm) can be attributed to the increase in RI when transferring the particles from buffer into the hydrogels, while the reduction in signal intensity is a result of the absorption and scattering by the hydrogels combined with a dilution of structures within the beam area. Casting the Al(III):g-cHOPO-

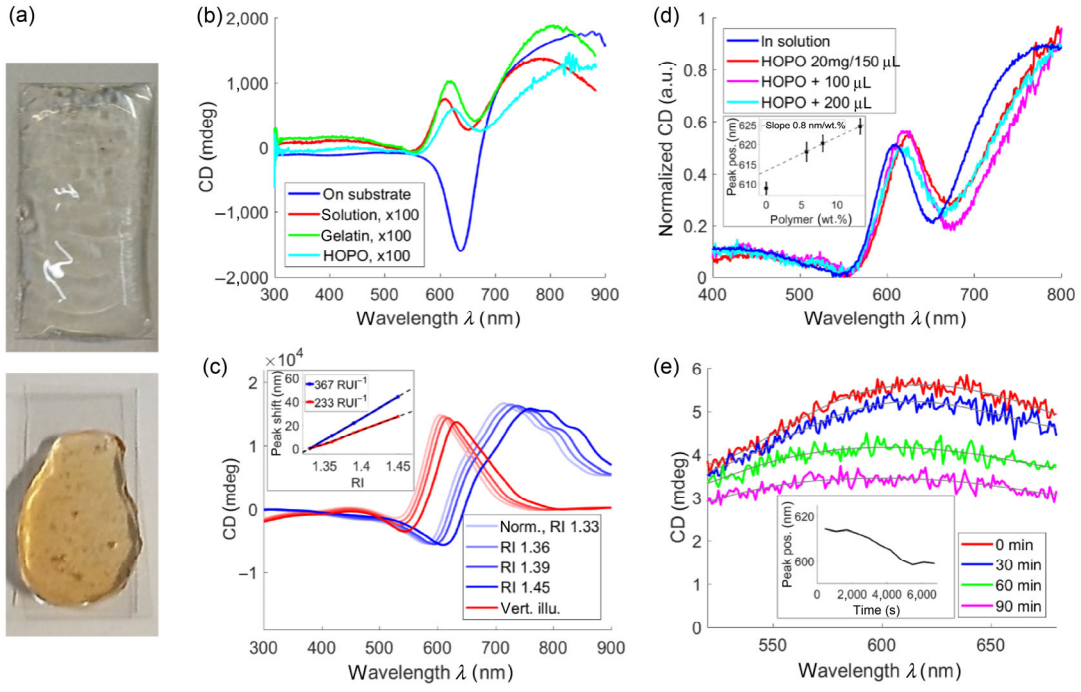

Figure 6 Integrating the lifted-off nano-hooks into hydrogels. (a) Pictures of the nano-hooks in gelatin (left) and in Al(III):g-cHOPO-PAH (right) hydrogels. (b) Comparing the CD signal of the sample, in solution (HEPES buffer), in gelatin and in Al(III):g-cHOPO-PAH. The lift-off leads to a flip of the lower λ peak, hydrogel integration leads to a red-shift due to the change in RI. Note the amplification for solution and hydrogel samples. (c) FDTD simulations on the effect of a change in bulk RI on the CD response. The peak positions were tracked (at the maxima seen in the shown spectral range) for the two illumination directions with the strongest and the weakest CD signal (see Fig. 4), averaging to a sensitivity of 300 RIU-1. (d) Comparing the CD peak position (at ~ 600 nm) for the hooks in solution and in Al(III):g-cHOPO-PAH hydrogels with increasing water content. Data normalized in CD amplitude for comparison (division with integral, original data in Fig. S3 in the ESM). The peak shift correlates well to the wt.% of polymer (see inset). (e) Tracking the CD peak shift induced by swelling of Al(III):g-cHOPO-PAH. The time-dependent peak-position is shown in the inset and was determined by maxima of 6th order polynomial fits to the raw data (grey solid lines) and binning of 7 measurements per point.

PAH hydrogel with different weight percentages (wt.%) of polymer leads to a shift in the LSPR peak (Fig. 6(d)). This shift correlates well with the polymer concentration (see inlay), showing that the integration of plasmonic NPs into hydrogels can be used for the remote sensing of the hydrogel's water content, which is especially useful for hydrogel systems like Al(III):g-cHOPO-PAH, where the crosslinking can be dynamically tuned. It should be noted that the slope of the peak shift does not go through the 0 wt.% point, suggesting that the NPs are themselves a crosslinking point for the polymer. The potential to dynamically study gel properties was tested by placing the gel in a cuvette filled with HEPES buffer and tracking the CD peak-shift during the swelling process of the gel, shown in Fig. 6(e). The peak continually shifts from 617 (±2) to 600 (±4) nm, indicating an increase in water content that reduces the wt.% of the polymer content by 21%.

Figure S3 in the ESM compares the CD spectra shown in Fig. 6(b), to extinction spectra with unpolarized light. The details of the measurements are given in the ESM; the results show the advantage of the chiral spectra: While the extinction of the hydrogels suppresses the signal of the LSPR peak for direct extinction measurements, the CD signal, for the same NP concentration, are sharp peak and usable e.g. for sensing purposes.

The successful integration of Au nanostructures into the self-healing Al(III):cHOPO-PAH hydrogel is a first time proof-of-principle for the combination of this novel class of hydrogels with functional NPs and offers opportunities for improving the structural and dynamic properties of this class of hydrogels while also having potential for injectable drug delivery applications [46, 47].

3 Conclusions

In conclusion, we were able to show the high versatility of the HMCL approach for the precise fabrication of chiral Au NPs. Furthermore, we demonstrated a novel way of transferring Au nano-hooks from SiO_2 substrates into aqueous and ethanol solutions, controlled by O_2 plasma oxidation and not involving strong acids or other hazardous liquids. Lastly, we performed a proof-of-principle experiment of the integration of chiral plasmonic elements into the reversibly cross-linked, self-healing Al(III):*g*-cHOPO-PAH hydrogel to form 3D, shaped and reconfigurable plasmonic metamaterials. In combination and for themselves these methods can have potential benefits for various applications from integrated photonics to biosensors and chiral catalysis.

4 Methods

4.1 Materials

Sample substrates were either 0.2 mm thick glass slides (Menzel-Gläser) for spectroscopic measurements or polished Si wafers for SEM measurements. The HMCL process involved polymethylmethacrylate (PMMA) (M_W = 495,000, 4% in anisole, purchased from Micro resist technology GmbH), poly(diallyldimethylammonium chloride) (PDDA, M_W = 200,000–350,000, 20% in H_2O, Sigma-Aldrich), poly(sodium-4-styrenesulfonate) (PSS, M_W = 70,000, 30% in H_2O, Sigma-Aldrich) and polyammonium chloride (PAX-XL60m Kemira Miljø). Colloidal polystyrene sulfate latex (PS) particles were purchased from Invitrogen (80–120 nm, approx. 5% coefficient of variation, 8.1% solids w/v).

4.2 Sample fabrication

Before fabrication substrates were cleaned either by wiping with acetone followed by 15 min in O_2-plasma (Vision 300 MK II, Advanced Vacuum) at RF power of 100 W, 300 mbar pressure and 55 cm^3/s

oxygen flow. An approximately 160 nm thick PMMA layer was deposited by a 1 min spincoating procedure at 3,000 rpm with an acceleration of 1,000 rpm/s followed by a 2 min baking step at 180 °C. Then, a 5 min ultraviolet (UV) ozone treatment (UV/Ozone ProCleanerTM Plus from Bioforce Nanosciences) was followed by the successive formation of self-assembled monolayers (SAMs) of PDDA, PSS and PAX, in that order, from diluted solutions (PDDA 2 wt.% in MilliQ water (MQ), PSS 2 wt.% in MQ, PAX 5 wt.% in MQ). The layers were formed by keeping the samples for 30 s in solution and rinsing it afterwards with MQ for 1 min and drying the sample in a flow of nitrogen gas. The SAMs helped stabilizing the following formation of a monolayer of PS particles, deposited from 0.2 wt.% solution for 2 min finalized by 90 s rinsing with MQ, drying in a nitrogen stream and 90 s UV ozone treatment.

The hole-mask was formed by PVD deposition of 20 nm Ti (E-beam thermal PVD, prototype, Polyteknik) with subsequent PS particle removal via tape stripping and O_2 plasma etching for 22 min (RF 50 W, 25 mbar pressure, 40 cm^3/s oxygen flow).

Directly after the etching step the samples were transferred into the PVD machine. The here presented chiral hook structures were achieved by PVD (1 Å/s) of Au at an angle between 12° and 32° while simultaneously rotating the sample holder. The rotation speed was either kept constant, accelerated (starting at 0.07 °/s and constantly accelerated until 0.25 °/s, it was kept for the last 50° for a total rotation of 270° and a total deposition of 209 nm Au) or deccelrated (starting at 0.25 °/s for the first 50° and then constantly decreased to 0.07 °/s for a total rotation of 270° and a total deposition of 209 nm Au).

After the Au deposition the sacrificial PMMA layer was removed in a > 2 min acetone ultrasonication step and ultrasonic cleaning in ethanol/IPA and MQ for 30s.

4.3 Lift off

First, a prolonged O_2 plasma treatment (RF 100 W, 30 mbar pressure, 55 cm^3/s oxygen flow) is used to create a stable layer of oxidized gold. Then, the sample is immersed in a solution with strong reducing agent, here either the strong ionic buffer HEPES (10 mM, 100 mM NaOH, pH 7.4, Sigma-Aldrich) or 1-dodecanethiols (10 mg/mL, Sigma-Aldrich) in ethanol (> 99.5 vol.%).

4.4 Hydrogel integration

Gelatin (bovine, Sigma-Aldrich) gels were cast by dissolving porcine gelatin at 10 wt.% in HEPES buffer at 55 °C in the NP suspension and then letting the solution cool down back to room temperature. Al(III):g-cHOPO-PAH hydrogel was fabricated by dissolving 20 mg of the g-cHOPO-PAH ((1-(2′carboxyethyl)-2-methyl-3-hydroxy-4(1H)-pyridinone-grafted polyallylamine hydrochloride, for protocol see [43]) in 30 µL HEPES buffer, followed by adjustment of the pH to 7.4 by adding 10 µL of 5 M NaOH and further dilution with 100 µL of the colloidal suspension. Reversible crosslinking was facilitated by the addition of 10 µL 0.5 mM aluminum chloride hexahydrate, which coordinates cHOPO above pH ~ 4. Before the hydrogel casting, the concentration of the hook solutions was increased by a factor of 4 by centrifugation (15 min, 15,000*g*) and removal of the top ¾ of liquid, followed by vortex mixing and ultrasonication. For the swelling experiment, the lift off was performed in dodecane-thiol solution followed by centrifugation and transferal of the concentrated suspended hooks into HEPES buffer. After another centrifugation step the concentrated hooks (now in HEPES) were integrated into Al(III):g-cHOPO-PAH hydrogel as described above.

4.5 CD and unpolarized light UV–Vis spectroscopy

Spectroscopic analysis with CPL was performed with a commercial CD spectrometer (Jasco-810 and Chirascan CD spectrophotometer). Spectra with unpolarized light were recorded with a custom build fiber spectrometer (CypherTM PDA spectrometer from B&WTek, range 350 nm to 1050 nm) with a 20 W constant current tungsten light source (BPS2.0, B&WTek).

4.6 Simulations

Simulations were carried out using the commercial FDTD solver lumerical solutions. For Au the dielectric function from Johnson & Christie was used, for the glass substrate and the surrounding medium constant RI values were set (Nglass = 1.52). In each case a mesh size of 2 nm × 2 nm × 2 nm was used and two perfectly matched layers at each side of the simulated cube.

4.7 SEM and XPS measurements

The SEM images presented here were obtained with the FEI Magellan 400 system, at an acceleration of 5 kV and a probe current of 50 pA. X-ray photon spectroscopy (XPS) data was collected with a Kratos Axis UltraDLD. The X-ray source is monochromated Al kα ($h\nu$ = 1,486.6 eV) and operates at 15 mA (150 W) and 10 kV. The pressure in the chamber was kept below 5×10^{-9} mbar during measurements. The high resolution spectra for Au 4f were obtained with pass energy of 20 eV. The deconvolution of the spectra was carried out using the software CasaXPS. The gold peaks have been deconvoluted with asymmetrical 95% Lorentzian [A(0.4,0.1,0)Gl(95)] peak shape for Au(0) and symmetrical 95% Lorentzian peak shape for Au(III).

Acknowledgements

This work was supported by the Independent Research Fund Denmark through grant DFF – 4184-00301 and by the Lundbeck Foundation through grant R180-2014-3468. Affiliation with the center for integrated materials research (iMAT) at Aarhus University is gratefully acknowledged.

Electronic Supplementary Material: Supplementary material (additional SEM and AFM images illustrating the effect of the oxygen plasma treatment on the hook structure and the blurring effect as well as on the lift-off process, FDTD simulated spectra comparing the hook on a substrate and in solution) is available in the online version of this article at https://doi.org/10.1007/s12274-019-2412-x.

References

[1] De Abajo, F. J. G. Nonlocal effects in the plasmons of strongly interacting nanoparticles, dimers, and waveguides. *J. Phys. Chem. C* **2008**, *112*, 17983–17987.

[2] McMahon, J. M.; Gray, S. K.; Schatz, G. C. Nonlocal optical response of metal nanostructures with arbitrary shape. *Phys. Rev. Lett.* **2009**, *103*, 097403.

[3] Alvarez, M. M.; Khoury, J. T.; Schaaff, T. G.; Shafigullin, M. N.; Vezmar, I.; Whetten, R. L. Optical absorption spectra of nanocrystal gold molecules. *J. Phys. Chem. B* **1997**, *101*, 3706–3712.

[4] Narayanan, R.; El-Sayed, M. A. Catalysis with transition metal nanoparticles in colloidal solution: Nanoparticle shape dependence and stability. *J. Phys. Chem. B* **2005**, *109*, 12663–12676.

[5] Romo-Herrera, J. M.; Alvarez-Puebla, R. A.; Liz-Marzán, L. M. Controlled assembly of plasmonic colloidal nanoparticle clusters. *Nanoscale* **2011**, *3*, 1304–1315.

[6] Huang, X. H.; Neretina, S.; El-Sayed, M. A. Gold nanorods: From synthesis and properties to biological and biomedical applications. *Adv. Mater.* **2009**, *21*, 4880–4910.

[7] De, M.; Ghosh, P. S.; Rotello, V. M. Applications of nanoparticles in biology. *Adv. Mater.* **2008**, *20*, 4225–4241.

[8] Grzelczak, M.; Pérez-Juste, J.; Mulvaney, P.; Liz-Marzán, L. M. Shape control in gold nanoparticle synthesis. *Chem. Soc. Rev.* **2008**, *37*, 1783–1791.

[9] Pérez-Juste, J.; Pastoriza-Santos, I.; Liz-Marzán, L. M.; Mulvaney, P. Gold nanorods: Synthesis, characterization and applications. *Coord. Chem. Rev.* **2005**, *249*, 1870–1901.
[10] Jana, N. R.; Gearheart, L.; Murphy, C. J. Wet chemical synthesis of high aspect ratio cylindrical gold nanorods. *J. Phys. Chem. B* **2001**, *105*, 4065–4067.
[11] Smith, D. K.; Korgel, B. A. The importance of the CTAB surfactant on the colloidal seed-mediated synthesis of gold nanorods. *Langmuir* **2008**, *24*, 644–649.
[12] Bohren, C. F.; Huffman, D. R. *Absorption and Scattering of Light by Small Particles*; Wiley: New York, 1998.
[13] Kelly, K. L.; Coronado, E.; Zhao, L. L.; Schatz, G. C. The optical properties of metal nanoparticles: The influence of size, shape, and dielectric environment. *J. Phys. Chem. B* **2003**, *107*, 668–677.
[14] Morales-Dalmau, J.; Vilches, C.; De Miguel, I.; Sanz, V.; Quidant, R. Optimum morphology of gold nanorods for light-induced hyperthermia. *Nanoscale* **2018**, *10*, 2632–2638.
[15] Novak, J. P.; Feldheim, D. L. Assembly of phenylacetylene-bridged silver and gold nanoparticle arrays. *J. Am. Chem. Soc.* **2000**, *122*, 3979–3980.
[16] Bidault, S.; García De Abajo, F. J.; Polman, A. Plasmon-based nanolenses assembled on a well-defined DNA template. *J. Am. Chem. Soc.* **2008**, *130*, 2750–2751.
[17] Brown, L. V.; Sobhani, H.; Lassiter, J. B.; Nordlander, P.; Halas, N. J. Heterodimers: Plasmonic properties of mismatched nanoparticle pairs. *ACS Nano*, **2010**, *4*, 819–832.
[18] Rycenga, M.; Camargo, P. H. C.; Li, W. Y.; Moran, C. H.; Xia, Y. N. Understanding the SERS effects of single silver nanoparticles and their dimers, one at a time. *J. Phys. Chem. Lett.* **2010**, *1*, 696–703.
[19] McPeak, K. M.; Van Engers, C. D.; Bianchi, S.; Rossinelli, A.; Poulikakos, L. V.; Bernard, L.; Herrmann, S.; Kim, D. K.; Burger, S.; Blome, M. et al. Ultraviolet plasmonic chirality from colloidal aluminum nanoparticles exhibiting charge-selective protein detection. *Adv. Mater.* **2015**, *27*, 6244–6250.
[20] Kuzyk, A.; Schreiber, R.; Fan, Z. Y.; Pardatscher, G.; Roller, E. M.; Högele, A.; Simmel, F. C.; Govorov, A. O.; Liedl, T. DNA-based self-assembly of chiral plasmonic nanostructures with tailored optical response. *Nature* **2012**, *483*, 311–314.
[21] Li, Q. Y.; Lu, G. X. Controlled synthesis and photocatalytic investigation of different-shaped one-dimensional titanic acid nanomaterials. *J. Power Sources* **2008**, *185*, 577–583.
[22] Chen, X. B.; Mao, S. S. Titanium dioxide nanomaterials: Synthesis, properties, modifications, and applications. *Chem. Rev.* **2007**, *107*, 2891–2959.
[23] Polavarapu, L.; Xu, Q. H. Water-soluble conjugated polymer-induced self-assembly of gold nanoparticles and its application to SERS. *Langmuir* **2008**, *24*, 10608–10611.
[24] Li, Z. T.; Zhu, Z. N.; Liu, W. J.; Zhou, Y. L.; Han, B.; Gao, Y.; Tang, Z. Y. Reversible plasmonic circular dichroism of Au nanorod and DNA assemblies. *J. Am. Chem. Soc.* **2012**, *134*, 3322–3325.
[25] Liu, W. J.; Zhu, Z. N.; Deng, K.; Li, Z. T.; Zhou, Y. L.; Qui, H. B.; Gao, Y.; Che, S. N.; Tang, Z. Y. Gold nanorod@Chiral mesoporous silica core-shell nanoparticles with unique optical properties. *J. Am. Chem. Soc.* **2013**, *135*, 9659–9664.
[26] Wang, Z. L. The new field of nanopiezotronics. *Mater. Today* **2007**, *10*, 20–28.
[27] Delclos, T.; Aimé, C.; Pouget, E.; Brizard, A.; Huc, I.; Delville, M. H.; Oda, R. Individualized silica nanohelices and nanotubes: Tuning inorganic nanostructures using lipidic self-assemblies. *Nano Lett.* **2008**, *8*, 1929–1935.
[28] Qiao, Y.; Wang, Y. J.; Yang, Z. Y.; Lin, Y. Y.; Huang, J. B. Self-templating of metal-driven supramolecular self-assembly: A general approach toward 1D inorganic nanotubes. *Chem. Mater.* **2011**, *23*, 1182–1187.
[29] Gansel, J. K.; Thiel, M.; Rill, M. S.; Decker, M.; Bade, K.; Saile, V.; von Freymann, G.; Linden, S.; Wegener, M. Gold helix photonic metamaterial as broadband circular polarizer. *Science* **2009**, *325*, 1513–1515.
[30] Radke, A.; Gissibl, T.; Klotzbücher, T.; Braun, P. V.; Giessen, H. Three-dimensional bichiral plasmonic crystals fabricated by direct laser writing and electroless silver plating. *Adv. Mater.* **2011**, *23*, 3018–3021.
[31] Guo, L. J. Nanoimprint lithography: Methods and material requirements. *Adv. Mater.* **2007**, *19*, 495–513.
[32] Hulteen, J. C.; Van Duyne, R. P. Nanosphere lithography: A materials general fabrication process for periodic particle array surfaces. *J. Vac. Sci. Technol. A* **1995**, *13*, 1553–1558.
[33] Verre, R.; Shao, L.; Odebo Länk, N.; Karpinski, P.; Yankovich, A. B.; Antosiewicz, T. J.; Olsson, E.; Käll, M. Metasurfaces and colloidal suspensions composed of 3D chiral Si nanoresonators. *Adv. Mater.* **2017**, *29*, 1701352.
[34] Verre, R.; Odebo Länk, N.; Andrén, D.; Šípová, H.; Käll, M. Large-scale fabrication of shaped high index dielectric nanoparticles on a substrate and in solution. *Adv. Opt. Mater.* **2018**, *6*, 1701253.
[35] McPeak, K. M.; Van Engers, C. D.; Blome, M.; Park, J. H.; Burger, S.; Gosálvez, M. A.; Faridi, A.; Ries, Y. R.; Sahu, A.; Norris, D. J. Complex chiral colloids and surfaces via high-index off-cut silicon. *Nano Lett.* **2014**, *14*, 2934–2940.
[36] Fredriksson, H.; Alaverdyan, Y.; Dmitriev, A.; Langhammer, C.; Sutherland, D. S.; Zäch, M.; Kasemo, B. Hole-mask colloidal lithography. *Adv. Mater.* **2007**, *19*, 4297–4302.
[37] Frederiksen, M.; Sutherland, D. S. Direct modification of colloidal hole-masks for locally ordered hetero-assemblies of nanostructures over large areas. *Nanoscale* **2014**, *6*, 731–735.
[38] Frank, B.; Yin, X. H.; Schäferling, M.; Zhao, J.; Hein, S. M.; Braun, P. V.; Giessen, H. Large-area 3D chiral plasmonic structures. *ACS Nano* **2013**, *7*, 6321–6329.
[39] Fang, Y. R.; Verre, R.; Shao, L.; Nordlander, P.; Käll, M. Hot electron generation and cathodoluminescence nanoscopy of chiral split ring resonators. *Nano Lett.* **2016**, *16*, 5183–5190.
[40] Krogsgaard, M.; Nue, V.; Birkedal, H. Mussel-inspired materials: Self-healing through coordination chemistry. *Chem. —Eur. J.* **2016**, *22*, 844–857.
[41] Krogsgaard, M.; Behrens, M. A.; Pedersen, J. S.; Birkedal, H. Self-healing mussel-inspired multi-pH-responsive hydrogels. *Biomacromolecules* **2013**, *14*, 297–301.
[42] Holten-Andersen, N.; Harrington, M. J.; Birkedal, H.; Lee, B. P.; Messersmith, P. B.; Lee, K. Y. C.; Waite, J. H. pH-induced metal-ligand cross-links inspired by mussel yield self-healing polymer networks with near-covalent elastic moduli. *Proc. Natl. Acad. Sci. USA* **2011**, *108*, 2651–2655.
[43] Andersen, A.; Krogsgaard, M.; Birkedal, H. Mussel-inspired self-healing double-cross-linked hydrogels by controlled combination of metal coordination and covalent cross-linking. *Biomacromolecules* **2018**, *19*, 1402–1409.
[44] Takano, Y.; Takahashi, J. I.; Kaneko, T.; Marumo, K.; Kobayashi, K. Asymmetric synthesis of amino acid precursors in interstellar complex organics by circularly polarized light. *Earth Planet. Sci. Lett.* **2007**, *254*, 106–114.
[45] Thoniyot, P.; Tan, M. J.; Karim, A. A.; Young, D. J.; Loh, X. J. Nanoparticle–hydrogel composites: Concept, design, and applications of these promising, multi-functional materials. *Adv. Sci.* **2015**, *21*, 1400010.
[46] Wang, C.; Flynn, N. T.; Langer, R. Controlled structure and properties of thermoresponsive nanoparticle-hydrogel composites. *Adv. Mater.* **2004**, *16*, 1074–1079.
[47] Menyo, M. S.; Hawker, C. J.; Waite, J. H. Versatile tuning of supramolecular hydrogels through metal complexation of oxidation-resistant catechol-inspired ligands. *Soft Matter* **2013**, *9*, 10314–10323.
[48] Yesilkoy, F.; Flauraud, V.; Rüegg, M.; Kim, B. J.; Brugger. J. 3D nanostructures fabricated by advanced stencil lithography. *Nanoscale* 2016, *8*, 4945–4950.
[49] Kontio, J. M.; Simonen, J.; Tommila, J.; Pessa, M. Arrays of metallic nanocones fabricated by UV-nanoimprint lithography. *Microelectron. Eng.* **2010**, *87*, 1711–1715.
[50] Vazquez-Mena, O.; Villanueva, L. G.; Savu, V.; Sidler, K.; Langlet, P.; Brugger, J. Analysis of the blurring in stencil lithography. *Nanotechnology* **2009**, *20*, 415303.
[51] Yunker, P. J.; Still, T.; Lohr, M. A.; Yodh, A. G. Suppression of the coffee-ring effect by shape-dependent capillary interactions. *Nature* **2011**, *476*, 308–311.

[52] Deegan, R. D.; Bakajin, O.; Dupont, T. F.; Huber, G.; Nagel, S. R.; Witten, T. A. Capillary flow as the cause of ring stains from dried liquid drops. *Nature* **1997**, *389*, 827–829.
[53] Hendry, E.; Carpy, T.; Johnston, J.; Popland, M.; Mikhaylovskiy, R. V.; Lapthorn, A. J.; Kelly, S. M.; Barron, L. D.; Gadegaard, N.; Kadodwala, M. Ultrasensitive detection and characterization of biomolecules using superchiral fields. *Nat Nanotechnol* **2010**, *5*, 783–787.
[54] Liu, J. J. Optical properties of chiral plasmonic nanoparticles and mesoporous silicon nanowires. Ph.D. Dissertation, Hong Kong Baptist University, Hong Kong, China, 2017.
[55] García-Guirado, J.; Svedendahl, M.; Puigdollers, J.; Quidant, R. Enantiomer-selective molecular sensing using racemic nanoplasmonic arrays. *Nano Lett*. **2018**, *18*, 6279–6285.
[56] Kalinkin, A. V.; Smirnov, M. Y.; Bukhtiyarov, A. V.; Bukhtiyarov, V. I. XPS study of gold oxidation with nitrogen dioxide in model Au/C samples. *Kinet*. *Catal*. **2015**, *56*, 796–800.
[57] Stadnichenko, A. I.; Koshcheev, S. V.; Boronin, A. I. Oxidation of the polycrystalline gold foil surface and XPS study of oxygen states in oxide layers. *Moscow*. *Univ*. *Chem*. *Bull*. **2007**, *62*, 343–349.
[58] Juodkazis, K.; Juodkazytė, J.; Jasulaitienė, V.; Lukinskas, A.; Šebeka, B. XPS studies on the gold oxide surface layer formation. *Electrochem*. *Commun*. **2000**, *2*, 503–507.